Understanding photovoltaic energy losses under indoor lighting conditions

Behrang H. Hamadani[a] (iD)

AFFILIATIONS

Engineering Laboratory, National Institute of Standards and Technology, Gaithersburg, Maryland 20899, USA

[a]Author to whom correspondence should be addressed: behrang.hamadani@nist.gov

ABSTRACT

The external luminescence quantum yield as a function of solar cell current density when exposed to low indoor light was estimated based on absolute electroluminescence measurements and a self-consistent use of the electro-optical reciprocity relationship. By determining the luminescence yield at current densities corresponding to the cell operation at the maximum power point, we can compute energy losses corresponding to radiative and nonradiative recombination. Combined with other major energy losses, we can obtain a clear picture of the fundamental balance of energy within the cell when exposed to room light with a typical total illuminance of 1000 lx or less.

https://doi.org/10.1063/5.0017890

The rapidly growing interest in energy harvesting from indoor ambient lighting for applications such as powering internet-of-things devices[1–5] has raised the need to address a range of technical issues. Some of the issues that have been discussed in recent years[6–13] include the testing protocol for current vs voltage (I–V) measurements, the theoretical power conversion efficiency (PCE) of various photovoltaic (PV) technologies, and modeling the device behavior under variable indoor environmental conditions.[14,15] However, questions related to the fundamental energy loss mechanisms within the cell, when exposed to a low-irradiance indoor spectrum such as a light emitting diode (LED) light source, have not been addressed in sufficient detail. In single-junction solar cells within the confines of the Detailed Balance model, four main energy loss mechanisms can be identified when the cell is exposed to a light source:[16–18] transmission loss, thermalization loss, recombination losses, and junction loss. Transmission and thermalization losses, which account for incident energy lost to unabsorbed photons and energy lost to electrons thermalizing to the edge of the conduction band, respectively, are easily computed from the external quantum efficiency (EQE) and the incident light's photon flux. The junction loss describes how much energy is lost when a photogenerated charge carrier with an initial energy equal to the band gap energy, E_g, traverses across a junction experiencing a potential difference V. The computation of the recombination losses, however, which include contributions from both radiative and non-radiative recombination processes, is more complex.

It has been understood for some time that the electroluminescence (EL) measurement of solar cells, and their connection to the EQE of the cell through the well-known reciprocity relationship, provides valuable information regarding recombination losses in solar cells.[17,19–22] However, EL is generally performed as a relative measurement and its use as a quantitative tool has been limited. Recently, it was demonstrated that when EL is performed as an absolute measurement, i.e., every emitted photon is counted, it becomes a very powerful tool for determining the external radiative emission rates in solar cells. Knowledge of the radiative rates leads to a direct computation of the external luminescence quantum yield, Y_{ext}, I–V curves, and important energy loss parameters for solar cells.[23,24] The external luminescence yield is related to the internal optical losses, and it has been shown that in order to approach the Shockley–Queisser (SQ) limit of conversion efficiency, Y_{ext} has to approach unity.[25,26] Therefore, obtaining the Y_{ext} value of solar cells under low light operation is an important goal for understanding device performance under such conditions.

The previously reported absolute EL measurements have been used to compute device-related losses under the maximum power point (MPP) operation at air mass 0 (AM 0) or AM 1.5 standard reporting conditions (SRCs).[23,24] However, the reporting conditions are quite different for low irradiance artificial environments where the illumination source is typically a visible-spectrum light source, with an illuminance of 1000 lx or less and a total radiant power per unit area of less than 3 W/m². Therefore, in order for EL measurements to be useful in determining the radiative and non-radiative losses, EL must also be performed at extremely low current densities. This is a measurement challenge that cannot be easily performed to any arbitrarily low current density, and a combination of measurements and extrapolation is needed to estimate Y_{ext}. Here, we will show that by using an iterative process involving the reciprocity relationship, we can take

advantage of both the I–V curves of various solar cells at 1000 lx and the absolute EL measurements to construct the external luminescence yield as a function of current density, J, for each solar cell. Finally, we calculate the four major energy losses described above at the MPP and explain why certain nominal solar cells perform so differently under the same illumination condition.

Electroluminescence measurements were performed on four different types of single junction solar cells using a Grand-EOS hyperspectral[27,28] wide-field imaging system by Photon, etc.[29] Hyperspectral imaging provides both spatial and spectral information, in high resolution, all within a convenient image cube. The spectral EL emission profiles from an entire 20 mm × 20 mm field of view were obtained as a function of the injection current supplied by a source-measure unit. To process the data, the raw EL image cube (in counts) was subtracted from a dark background image cube where no current was sourced through the cell. Then, an average net count was computed over a large portion of the cell for each injection current. A spectral calibration factor was applied to the average net count to convert it to the absolute external radiative emission rate $R_{ext}(E)$ in units of photons/m^2 s eV as a function of the photon energy in eV. In order to obtain this calibration factor, we first calibrated a spectroradiometer against a NIST FEL lamp[30] by placing a pinhole aperture on one port of a small integrating sphere and connecting another port to the spectroradiometer using an optical fiber. Then, in a separate measurement, we input light from a quartz-tungsten halogen lamp into a second sphere and took hyperspectral images of the same pinhole (mounted on one of the ports) with light emanating out through its opening. By measuring the net count that the hyperspectral imager receives from the pinhole and also measuring the absolute irradiance at the pinhole port by the spectroradiometer, a spectral calibration factor for absolute EL measurements can be calculated. This calibration procedure is only performed once, and the resulting calibration factor is applied to all subsequent EL measurements on solar cells.

The I–V measurements were performed at room temperature (T = 22 °C) using a reference-cell-based method[31] under a warm white LED with a correlated color temperature (CCT) of 3000 K and a total illuminance of 1000 lx. EQE measurements were also separately performed on each cell using a differential spectral responsivity technique.[32–34] The measurement results of four different solar cells are presented here. The three cells labeled GaAs-2, GaInP, and Si are nominal 4 cm^2 gallium arsenide, gallium indium phosphide, and passivated emitter and rear contact (PERC) silicon cells diced from the wafer; the cell labeled GaAs-1 is a thin flexible gallium arsenide cell with a nominal area of 8.15 cm^2 by Alta Devices.[26,29,35] The AM 1.5 global SRC performances as captured in the PCE of these devices are ≈ 25.2%, 23.9%, 15.6%, and 20.8% for the GaAs-1, GaAs-2, GaInP, and Si cells, respectively. However, the PCE results under the low light CCT-3000 K LED spectrum with a total irradiance of 2.93 W/m^2 change to 35.2%, 22.8%, 27.1%, and 14.1% for the same four cells in order. The current density vs voltage (J–V) curves of all four devices under this low light condition and the irradiance of the LED source are plotted in Fig. 1, where the symbols are measurement data and the solid curves are fits to the data as discussed later.

For the GaInP and Si cells, the changes in the PCE can generally be explained by the short circuit current density, J_{sc}, of each cell under the two different reporting conditions. The spectral shape of the EQE of the GaInP cell, for example, is well matched to the irradiance of a
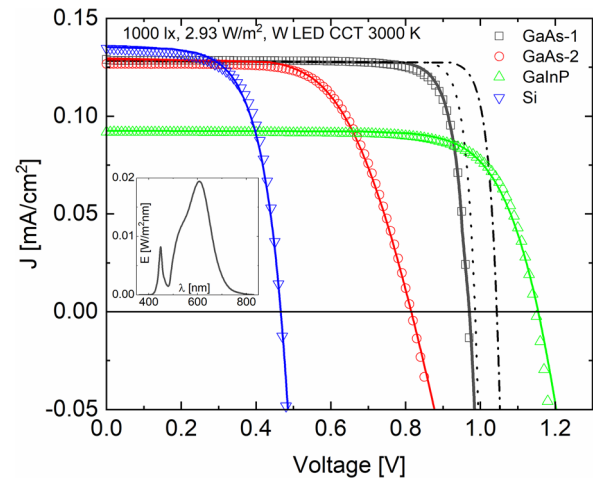

FIG. 1. (Inset) the spectral irradiance plot of the LED source (CCT 3000 K) used in our analysis. (main) measured J–V curves under the LED illumination (symbols). The solid curves are the reciprocity-derived J–V curves based on Y_{ext} values. The dotted curve is a J–V computation for the GaAs-1 cell with the assumption that Y_{ext} is fixed at 0.1 for all J values. The dashed-dotted curve is the same computation with Y_{ext} fixed at 1 (i.e., the SQ limit).

white LED source and can absorb a larger percentage of photons from an LED than from the sun, whereas in Si, this effect is reversed. The changes between the two GaAs cells, however, are more puzzling because the two cells have almost identical EQEs. Therefore, in order to understand the performance differences, we must first understand why the GaAs-1 cell has a higher voltage output than the GaAs-2 cell, particularly under low light conditions. We turned to our absolute EL measurements to extract the external luminescence quantum yield, $Y_{ext} \equiv q \int_{E_{min}}^{E_{max}} R_{ext}(E) dE / J_{inj} = q R_{ext}^{tot} / J_{inj}$, as a function of the injection current density, J_{inj}, and then used the carrier balance equation to compute this quantity as a function of the solar cell current J operated under the LED irradiance. Here, q is the electron charge in coulombs. With Y_{ext} determined, the radiative and non-radiative recombination losses can be calculated at the maximum power point voltage and current (V_m, J_m). All the other major losses can be computed separately with the help of band gap energies, E_g, and the EQE curves.

Figure 2 (main) shows a log-log plot of Y_{ext} vs J_{inj} for all four devices. From these plots, it is immediately evident that the GaAs-1 cell is the most efficient device for luminescent extraction, showing an efficiency of ≈ 10% at a low current density of 1 mA/cm^2. The luminescence yield of the GaAs-2 cell is significantly lower at the same current density and shows a very strong drop with decreasing J_{inj}. A similar behavior with much lower yields is evident for the GaInP and Si cells. With the stated goal of using these data to compute Y_{ext} vs J plots, we first examine the carrier balance equation,[24,36]

$$J_L + J = q R_{ext}^{tot}[J] + q R_{nr}[J] \equiv \frac{q R_{ext}^{tot}[J]}{Y_{ext}[J]}, \qquad (1)$$

where J_L is the light-generated current density given by $J_L = q \int_{E_{min}}^{E_{max}} \varphi_{LED}[E] EQE[E] dE$, φ_{LED} is the incident LED's photon flux, and R_{nr} is the rate of nonradiative emission. Note that all emission rates and the luminescence yield are current density dependent, as shown in Fig. 2, and we have included the [J] term to denote this
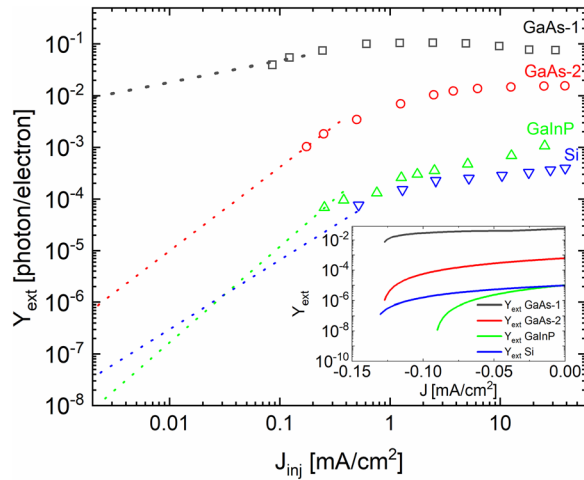
FIG. 2. (Main) measured external luminescence quantum yield vs injection current (symbols) for the four solar cells discussed in this work. Dotted lines are extrapolated Y_{ext} to very low current densities. (Inset): constructed external luminescence yields vs solar cell current density.

functional dependence. The solar cell current density is negative when the cell is operated under illumination (net extracted current), and so the relationship between J and J_{inj} is simply given by $J = J_{inj} - J_L$. Therefore, we can construct plots of Y_{ext} vs J using Eq. (1). With the J_L values for the four solar cells GaAs-1, GaAs-2, GaInP, and Si computed to be 0.128 mA/cm², 0.130 mA/cm², 0.0925 mA/cm², and 0.135 mA/cm², respectively, it can be seen that J_{inj} needs to be at least as low as these values for each cell to achieve $J = 0$ (i.e., Y_{ext} under open circuit conditions), but obviously to reach lower (negative) values such as $J = J_m$, Y_{ext} measurements at much lower injection current densities need to be performed.

Due to the sensitivity (signal to noise ratio) of the hyperspectral imaging system and the need to balance image acquisition times with spectral resolution, reliable EL data could only be obtained down to current densities in the range of ≈ 0.1 mA/cm²–0.4 mA/cm², depending on the luminescence yield. To estimate Y_{ext} at lower J_{inj}, we turn to a self-consistent extrapolation method. In the absence of a comprehensive physics-based model to guide us, this extrapolation needs to be performed in such a way that the resulting $Y_{ext}[J]$ function models the measured J–V curve data as well as possible. We performed this process iteratively, starting with a function of the form $y = ax^b$ fitted to the first few low J_{inj} data points of the Y_{ext} vs J_{inj} plot for each cell, to extract the a and b parameters. We then used the resulting $Y_{ext}[J_{inj}]$ to calculate $Y_{ext}[J]$. Then, the J–V curve can be calculated using the reciprocity relationship solved for $V[J]$,

$$V[J] = \frac{kT}{q} \ln \frac{R_{ext}^{tot}[J]}{\langle EQE \rangle_{EL} \int_{E_g}^{\infty} B[E]dE} + JAR_s, \quad (2)$$

where $B[E] \cong 2\pi E^2 h^{-3} c^{-2} \exp(-E/kT)$ is the spectral photon density of a black body, k is Boltzmann's constant, h is Planck's constant, T is the temperature of the cell, and c is the speed of light in a vacuum. The term $\langle EQE \rangle_{EL} = \int EQE[E]R_{ext}[E]dE / \int R_{ext}[E]dE$ is an average

EQE term over the EL emission spectral region. Here, we have included a voltage loss term due to a series resistance element, R_s, because we have noticed that certain devices such as the GaAs-2 and the GaInP cells have an unusually high series resistance under low light measurements. We verified this by a separate analysis where we fit the J–V curve data to the well-known double-diode model[37,38] and extracted various device parameters, including the series resistance. The values for R_s for each cell were fixed in the Eq. (2) calculation from this secondary analysis.

If the computed $V[J]$ curve using Eqs. (1) and (2) and based on the extrapolation for $Y_{ext}[J_{inj}]$ does not fit the J–V curve data, then the a and b parameters are slightly modified so that new $Y_{ext}[J]$ and $V[J]$ values are calculated and compared against the J–V data. The final result of this process is shown by the dotted lines in Fig. 2 down to the lowest J_{inj} values needed to compute the J–V curve from the open circuit voltage (V_{oc}) toward J_{sc}, including past the knee of the curve where the point (V_m, J_m) is located. These extrapolated plots show that Y_{ext} continues to drop precipitously at low injection currents for all devices except for the GaAs-1 cell, where the slope of the $Y_{ext}[J_{inj}]$ plot is much smaller than the rest. This observation indicates that luminescent extraction is extremely efficient for this particular cell even at very low current densities where the non-radiative Shockley–Read–Hall (SRH) recombination can dominate over all recombination mechanisms.[17]

Figure 2 (inset) shows the final constructed Y_{ext} vs J plots under the solar cell operation. These findings are consistent with previously reported results in thin-film GaAs cells.[24] The band gap energy for each cell was estimated from the inflection point in the long wavelength tail region of the EQE curve[22,39,40] and is listed in Table I. The good agreement between reciprocity-derived J–V curves (solid curves) and the actual measurements (symbols), shown in Fig. 1, validates our approach. We note that the J dependence of the $Y_{ext}[J]$ function as shown in Fig. 2 has a noticeable influence on the curvature (or the fill factor, FF) of the modeled J–V curves. So, in addition to a high series resistance, which generally lowers the FF, a decreasing Y_{ext} with an appreciable dependence on J reduces the fill factor even further, ultimately resulting in a smaller V_m and larger junction losses.

This point is demonstrated by the dotted black J–V curve in Fig. 1, which is a theoretical, reciprocity-derived J–V computed for the GaAs-1 cell with the assumption that $Y_{ext} = 0.1$ (fixed) for all J, while all other parameters are kept the same. This modeled J–V curve gives FF = 0.88, which is slightly larger than the experimental findings for the true $Y_{ext}[J]$ with FF = 0.82, and validates that Y_{ext} has a J dependence instead of a fixed value. The dashed-dotted curve is the theoretical J–V curve for the same cell assuming perfect luminescent extraction, i.e., $Y_{ext} = 1$, with the implication that all recombination events within the cell are radiative. The predicted PCE of 40.6% for the ideal J–V curve is consistent with the maximum efficiency predicted in the literature using first principles computations under indoor lighting.[6,18]

Additionally, the $Y_{ext}[J]$ measurements explain the differences between the two GaAs J–V curves. Since the voltage penalty[25] from the ideal SQ V_{oc} is given by $kT \ln(Y_{ext})$, ΔV_{oc} between the two curves should be given by

$$\Delta V_{oc} \cong E_g^{GaAs-1} + kT \ln(Y_{ext}^{GaAs-1}) - E_g^{GaAs-2} - kT \ln(Y_{ext}^{GaAs-2}). \quad (3)$$

While the voltage loss term for the GaAs-1 cell is only 73.3 mV below the SQ limit at the measurement temperature, this term

TABLE I. Energy loss fractions, normalized by the incident power, for all major loss mechanisms.

Cell ID	E_g (eV)	Rad loss	Nonrad. loss	Therm. loss	Trans. loss	Junc. loss	Output power	Total
GaAs-1	1.434	7.00×10^{-4}	0.041	0.372	0.000	0.235	0.352	1.0003
GaAs-2	1.385	1.68×10^{-6}	0.077	0.388	0.000	0.308	0.228	1.0010
GaInP	1.823	9.97×10^{-9}	0.061	0.364	0.064	0.244	0.271	1.0047
Si	1.095	6.11×10^{-8}	0.078	0.494	0.000	0.287	0.141	1.0004
GaAs-1 if $Y_{ext} = 1$	1.434	1.95×10^{-2}	0.000	0.372	0.000	0.203	0.406	1.0004

increases to 188 mV for the GaAs-2 cell. Equation (3) gives $\Delta V_{oc} = 163$ mV, which is very close to the experimentally observed difference of 155 mV. The highly efficient luminescent extraction from the GaAs-1 cell is ultimately rooted in its superior photonic design aimed at maximizing photon recycling in this device. In addition to growth of high-quality materials, the fabrication process of these cells includes surface texturing and a highly reflective back contact, steps that have been shown to reduce dark currents, increase photon recycling and the carrier concentration, and boost the solar cell V_{oc}.[26,35] Similarly, the voltage loss from ideal V_{oc} for both the GaInP and Si cells is ≈ 293 mV under our 1000 lx illumination condition. These observations suggest that nonradiative recombination can dominate the device performance, even for a direct band gap material such as GaInP under low light.

Finally, we summarize each cell's important photovoltaic energy losses in Table I, calculated from the Y_{ext} and EQE measurements under the LED's photon flux using the equations outlined in Table IV of Chen et al.[23] All the losses and the output power at the MPP have been normalized to the incident irradiance (2.93 W/m²). As a consistency check, we sum every row to make sure that it adds to unity. The most significant energy loss component is the thermalization loss accounting for anywhere from $\approx 37\%$ to 49% of the incident energy. The junction loss is also inevitable, but it depends significantly on V_{oc} and the fill factor of the cell. Between the two GaAs cells, 7.3% more incident energy is lost in GaAs-2 due to its lower V_m, which is related to both the lower luminescence efficiency and the higher series resistance. The direct nonradiative recombination losses, which are derived from the estimated Y_{ext} at the MPP, are in the range of 4–8% of the total incident energy. As expected, the GaAs-2 cell exhibits almost twice the nonradiative recombination as the GaAs-1 cell, consistent with its inferior electrical performance. Finally, the last row shows the losses for an ideal GaAs cell. For such an ideal cell, all nonradiative losses are 0, with emission-related recombination completely in the radiative regime with a loss value less than 2% and a further 3% reduction in the junction loss, hence delivering a maximum theoretical PCE of 40.6%.

In summary, we have shown that the external luminescence quantum yield of various solar cells can be estimated under indoor lighting conditions using a self-consistent method that utilizes the reciprocity relationship and absolute electroluminescence measurements. The stark differences in the luminescence yield of various cells help explain the variability in the electrical performance data of these cells particularly as regards the voltage output of the cells. Finally, the computation of the major energy loss terms under the maximum power point operation presents a clear picture of the energy flow within each cell when exposed to an artificial light source.

DATA AVAILABILITY

The data that support the findings of this study are available from the corresponding author upon reasonable request.

REFERENCES

[1]J. A. Paradiso and T. Starner, IEEE Pervasive Comput. **4**, 18 (2005).
[2]R. Haight, W. Haensch, and D. Friedman, Science **353**, 124 (2016).
[3]A. Nasiri, S. A. Zabalawi, and G. Mandic, IEEE Trans. Ind. Electron. **56**, 4502 (2009).
[4]M. Masoudinejad, J. Emmerich, D. Kossmann, A. Riesner, M. Roidl, and M. ten Hompel, in The Sixth International Renewable Energy Congress (2015).
[5]I. Mathews, S. N. R. Kantareddy, S. Sun, M. Layurova, J. Thapa, J. Correa-Baena, R. Bhattacharyya, T. Buonassisi, S. Sarma, and I. M. Peters, Adv. Funct. Mater. **29**, 1904072 (2019).
[6]M. Freunek, M. Freunek, and L. M. Reindl, IEEE J. Photovoltaics **3**, 59 (2013).
[7]N. H. Reich, W. G. J. H. M. van Sark, and W. C. Turkenburg, Renewable Energy **36**, 642 (2011).
[8]H. K. H. Lee, J. Wu, J. Barbé, S. M. Jain, S. Wood, E. M. Speller, Z. Li, F. A. Castro, J. R. Durrant, and W. C. Tsoi, J. Mater. Chem. A **6**, 5618 (2018).
[9]K. A. Haque and M. Z. Baten, AIP Adv. **9**, 055326 (2019).
[10]V. Bahrami-Yekta and T. Tiedje, Opt. Express **26**, 28238 (2018).
[11]I. Mathews, P. J. King, F. Stafford, and R. Frizzell, IEEE J. Photovoltaics **6**, 230 (2016).
[12]Y. Afsar, J. Sarik, M. Gorlatova, G. Zussman, and I. Kymissis, in 38th IEEE Photovoltaic Specialists Conference (2012), p. 001948.
[13]B. Minnaert and P. Veelaert, Energies **7**, 1500 (2014).
[14]A. Fajardo Jaimes and F. Rangel de Sousa, Sol. Energy **157**, 792 (2017).
[15]M. Masoudinejad, J. Emmerich, D. Kossmann, A. Riesner, M. Roidl, and M. ten Hompel, Sustainable Cities Soc. **25**, 74 (2016).
[16]F. H. Alharbi and S. Kais, Renewable Sustainable Energy Rev. **43**, 1073 (2015).
[17]T. Kirchartz and U. Rau, Phys. Status Solidi **205**, 2737 (2008).
[18]G. Jarosz, R. Marczyński, and R. Signerski, Mater. Sci. Semicond. Process. **107**, 104812 (2020).
[19]T. Kirchartz, A. Helbig, W. Reetz, M. Reuter, J. H. Werner, and U. Rau, Prog. Photovoltaics Res. Appl. **17**, 394 (2009).
[20]R. Hoheisel, D. Scheiman, S. Messenger, P. Jenkins, and R. Walters, IEEE Trans. Nucl. Sci. **62**, 2894 (2015).
[21]A. Delamarre, L. Lombez, and J. F. Guillemoles, Proc SPIE **8256**, 825614 (2012).
[22]T. Kirchartz, V. Huhn, A. Gerber, B. E. Pieters, and U. Rau, in Advanced Characterization Techniques for Thin Film Solar Cells (Wiley-VCH Verlag GmbH & Co. KGaA, Weinheim, Germany, 2016), pp. 71–92.

[23]S. Chen, L. Zhu, M. Yoshita, T. Mochizuki, C. Kim, H. Akiyama, M. Imaizumi, and Y. Kanemitsu, Sci. Rep. **5**, 7836 (2015).

[24]X. Hu, T. Chen, J. Xue, G. Weng, S. Chen, H. Akiyama, and Z. Zhu, IEEE Photonics J. **9**, 8400409 (2017).

[25]O. D. Miller, E. Yablonovitch, and S. R. Kurtz, IEEE J. Photovoltaics **2**, 303 (2012).

[26]E. Yablonovitch, O. D. Miller, and S. R. Kurtz, in The 38th IEEE Photovoltaic Specialists Conference (2012), Vol. 3, p. 001556.

[27]E. Gaufrès, S. Marcet, V. Aymong, N. Y.-W. Tang, A. Favron, F. Thouin, C. Allard, D. Rioux, N. Cottenye, M. Verhaegen, and R. Martel, J. Raman Spectrosc. **49**, 174 (2018).

[28]M. Verhaegen, S. Lessard, and S. Blais-Ouellette, Proc. SPIE **8374**, 83740G (2012).

[29]Certain commercial equipment, instruments, software, or materials are identified in this paper to specify the experimental procedure adequately. Such identification is not intended to imply recommendation or endorsement by the National Institute of Standards and Technology nor is it intended to imply that the materials or equipment identified is necessarily the best available for the purpose.

[30]H. W. Yoon and C. Gibson, NIST Special Publications (U.S. Department of Commerce, 2011), Vol. 250-89.

[31]B. H. Hamadani and M. B. Campanelli, IEEE J. Photovoltaics **10**, 1119 (2020).

[32]J. Roller and B. H. Hamadani, Appl. Opt. **58**, 6173 (2019).

[33]B. H. Hamadani, J. Roller, B. Dougherty, F. Persaud, and H. W. Yoon, Appl. Opt. **52**, 5184 (2013).

[34]B. H. Hamadani, J. Roller, A. M. Shore, B. Dougherty, and H. W. Yoon, Appl. Opt. **53**, 3565 (2014).

[35]B. M. Kayes, H. Nie, R. Twist, S. G. Spruytte, F. Reinhardt, I. C. Kizilyalli, and G. S. Higashi, in The 37th IEEE Photovoltaic Specialists Conference (2011).

[36]J. Jia, Y. Miao, Y. Kang, Y. Huo, M. Mazouchi, Y. Chen, L. Zhao, H. Deng, P. Supaniratisai, S. H. AlQahtani, and J. S. Harris, Opt. Express **23**, A219 (2015).

[37]O. Breitenstein, Semicond. Semimetals **89**, 1 (2013).

[38]J. P. Babaro, K. G. West, and B. H. Hamadani, Energy Sci. Eng. **4**, 372 (2016).

[39]T. Gershon, B. Shin, N. Bojarczuk, T. Gokmen, S. Lu, and S. Guha, J. Appl. Phys. **114**, 154905 (2013).

[40]T. Kirchartz, U. Rau, M. Kurth, J. Mattheis, and J. H. Werner, Thin Solid Films **515**, 6238 (2007).